



Equivalent electrical circuit framework for nonlinear and high quality factor piezoelectric structures[☆]



Tarcísio M.P. Silva^a, Marcel A. Clementino^a, Alper Erturk^b, Carlos De Marqui Jr^{a,*}

^a Department of Aeronautical Engineering, Sao Carlos School of Engineering, University of Sao Paulo, Sao Carlos, SP 13566-590, Brazil

^b G. W. Woodruff School of Mechanical Engineering, Georgia Institute of Technology, Atlanta, GA 30332-0405, USA

ARTICLE INFO

Keywords:

Equivalent circuit
Nonlinear
Piezoelectric structures
High quality factor

ABSTRACT

Equivalent electrical circuits are useful simulation tools to emulate and investigate the behavior of electro-mechanically coupled systems and structures as well as to develop energy harvesting or control circuits, among other configurations with two-way coupling. The existing efforts in this context have mostly considered linear structural (mechanical) domain, occasionally with nonlinear circuit for signal process and control. Typically, resonant circuits are employed to represent the mechanical domain of single- or multi-degree-of-freedom systems, while ideal transformers or current- and voltage-dependent sources are employed to model the electro-mechanical coupling. However, practical limitations of ideal transformers and dependent sources are challenges for experimental implementations of equivalent circuits. Furthermore, the internal resistance of equivalent resonant circuits limits the representation of high quality factor systems. This paper introduces equivalent electrical circuits for linear and nonlinear electromechanically coupled systems with high quality factor and various types of nonlinearities. The focus is placed on piezoelectric structures that exhibit stiffness and damping nonlinearities. An alternative to the existing models for the electromechanical coupling is also presented for convenient simulation of coupled system dynamics using standard electronic simulation programs. The equivalent circuit framework given here for high quality factor electromechanical systems is validated against both linear and nonlinear case studies, including published data for a nonlinear piezoelectric energy harvester. The proposed framework paves the way for the design of circuits emulating nonlinear structures, such as nonlinear vibration absorbers and sinks.

1. Introduction

Equivalent electrical circuit representations of electromechanical systems and structures have been used in numerous research domains from vibration control [1,2] to energy harvesting [3–6], while the present work is predominantly focused on piezoelectric energy harvesting and the literature review will be limited to that. The research field of vibration-based energy harvesting has been investigated by several research groups over the last decade [7–9]. The goal is to enable self-powered systems by converting the waste vibration energy available in their environments into usable electrical energy. Although different transduction mechanisms (piezoelectric [7,8,10–13], electromagnetic [14–18] and electrostatic [10,19,20]) have been suggested for converting vibrations to electricity, piezoelectric energy harvesting has received the most attention due to the high power density and ease of application of piezoelectric materials [8,21–23].

Linear resonant piezoelectric energy harvesters have been extensively studied and well understood [11,12], and more recently there has been growing interest in the modeling and leveraging mechanical nonlinearities [24] (which is separate from the leveraging of nonlinear electrical signal processing). The motivation in nonlinear energy harvesting is to exploit nonlinear phenomena to provide broadband energy harvesters, overcoming the main limitation of linear resonant energy harvesters (that are effective only at resonance excitation usually with a narrow bandwidth). The existing literature includes various nonlinear energy harvesters with intentionally designed nonlinearities [25–28] and several review papers [29–31] can be found for examples of nonlinear and other methods of broadband energy harvesting. In a recent effort, Leadenham and Erturk [32,33] presented the modeling and experimental validations of an M-shaped oscillator for broadband energy harvesting. The M-shaped configuration is an alternative to complex forms of symmetric Duffing oscillators and its flexible asymmetric

[☆] This paper was recommended for publication by Associate Editor Dr. M Moallem.

* Corresponding author.

E-mail address: demarqui@sc.usp.br (C. De Marqui).

nonlinear behavior yields broadband behavior under low excitation levels (as low as mill-g vibration levels). Furthermore, enhanced electrical power output was reported since the M-shaped structure made from spring steel is a high quality factor device (this strongly nonlinear configuration will be visited as a case study in the present work).

Most of the papers on linear and nonlinear energy harvesting have considered a simple load resistance in the electrical domain of the problem in order to estimate the electrical power output of the harvesters. However, charging a storage component requires a stable output voltage and efficient electrical circuits for linear and nonlinear energy harvesting devices. Another body of literature also includes standard AC-DC converters (as a one stage energy harvesting interface) [34], two-stage energy harvesting circuits that includes DC-DC conversion for impedance matching [35,36], and also synchronized switching circuits for piezoelectric energy harvesting [37,38]. Simulation of piezoelectric energy harvesters with more complex interface circuits requires implementing equivalent circuit models in circuit simulation software. Therefore, researchers have also presented equivalent circuit models for single- or multiple-degree-of-freedom (SDOF or MDOF) linear and nonlinear piezoelectric energy harvesting systems [3–6].

An early effort on the equivalent electrical representation of SDOF and MDOF linear electromechanically coupled systems was presented by Elvin and Elvin [3]. In another paper [4], the same authors described a coupled finite element – SPICE model of a linear electromechanically coupled system. Bayik et al. [6] presented an equivalent circuit for a piezo-patch energy harvester on a thin plate with AC-DC conversion. Equivalent circuit representations of the aforementioned papers [3–6] are limited to structurally (i.e. mechanically) linear systems with linear coupling since they are based on the modal decomposition of the DOFs of the electromechanically coupled system. To overcome this limitation, Elvin [5] presented two approaches to obtain the equivalent electrical representation of linear and nonlinear electromechanically coupled systems. First, system-level circuits approach is employed to model the harvester behavior. Then, dependent voltage equivalent circuits are employed to represent the nonlinear system.

Challenges remain for the practical implementation of equivalent circuits in the presence of nonlinearities. Most of the papers on equivalent electrical representation consider a resistive-inductive-capacitive (RLC) circuit as the equivalent of the mechanical domain of the problem while ideal transformers or voltage-dependent sources provide the forward and backward electromechanical coupling effects. The equivalent electrical representation of high quality factor mechanical and electromechanical systems would demand RLC circuits with extremely low internal resistance values (typically on the order of a few m Ω). In practice, however, such internal resistance is lower than the individual internal resistances of inductors and capacitors. Therefore, typical RLC circuits are unsuitable for the appropriate practical electrical representation of high quality factor devices. Furthermore, the representation of the electromechanical coupling effects by an ideal transformer cannot be obtained in practice, although they have been considered in standard electronic simulation programs.

In this paper, a novel nonlinear equivalent electrical circuit framework for SDOF linear and nonlinear oscillators with electromechanical coupling is presented with a focus on nonlinear piezoelectric structures. The circuit is based on operational-amplifier (op-amp) sub-circuits of low internal resistance to represent high quality factor system dynamics. The proposed framework also allows for the inclusion of different sources of nonlinearities, such as nonlinear damping, as well as symmetric and asymmetric nonlinear stiffness terms of any order. Moreover, a new equivalent electrical representation for the forward and backward coupling (electromechanical coupling of the system) is also presented. The validation of the proposed circuit is presented in two cases. First, the equivalent electrical representation of a high quality factor linear SDOF mechanical system (mass-spring-damper system) is considered. The experimental results obtained from

breadboard implementation of the equivalent electrical circuit are compared with the numerical solution of the governing equation of the system. In the second case, the equivalent electrical representation of a SDOF nonlinear oscillator with electromechanical coupling is investigated. The experimental results obtained from breadboard implementation of the equivalent electrical circuit are validated against results from [33].

2. Components of the equivalent nonlinear circuit

The equivalent circuit is presented in this section as the electrical representation of a nonlinear SDOF oscillator with electromechanical coupling. Two different sources of nonlinearity are considered: nonlinear damping and nonlinear stiffness. Dissipative effects are assumed as a combination of linear viscous and quadratic damping (nonlinear dissipation) in the SDOF model. The other source of nonlinearity is nonlinear stiffness and the most general case of an n -order polynomial is considered in this section. The first-order coefficient is the linear stiffness for small displacements while the higher-order terms represent symmetric and asymmetric nonlinear stiffness terms. Therefore, the governing equations of the electromechanically coupled nonlinear oscillator are

$$m\ddot{z} + b_1\dot{z} + b_2(\dot{y} + \dot{z})|\dot{y} + \dot{z}| + F(z) - \theta V_p = -m^*\ddot{y} \quad (1a)$$

$$F(z) = k_1z + \sum_{n=2}^j k_n z^n \quad (1b)$$

$$C_p V_p + Q_p + \theta z = 0 \quad (1c)$$

where m is the equivalent mass of the structure, m^* is the effective mass that causes the forcing term due to base excitation ($m = m^*$ if the spring mass is negligible when compared to the lumped mass attachments), b_1 is the linear viscous damping coefficient, b_2 is the quadratic (velocity-squared) damping coefficient (used to model dissipation due to fluid-structure interaction), $F(z)$ is the nonlinear elastic restoring force, where k_1 the linear stiffness coefficient and j is the order of the nonlinear stiffness, θ is the equivalent electromechanical coupling, V_p is the voltage across the piezoelectric material, Q_p is the electric charge output from the piezoelectric material, z is the relative displacement between the lumped mass and the moving base, and y is the base displacement as the source of mechanical excitation. An over-dot stands for differentiation with respect to time.

Equations (1) are the basis for the equivalent electrical representation of nonlinear electromechanically coupled systems presented in this work. Base excitation is the typical scenario in vibration energy harvesting, while other forms of mechanical excitation can be easily accommodated in other scenarios, such as vibration control, using the following framework. The solution of Equations (1) based on a system-level approach requires the following representation:

$$m\ddot{z} = -b_1\dot{z} - b_2(\dot{y} + \dot{z})|\dot{y} + \dot{z}| - F(z) + \theta V_p - m^*\ddot{y} \quad (2a)$$

$$V_p = -\frac{Q_p}{C_p} - \frac{\theta z}{C_p} \quad (2b)$$

The equivalent circuit representation of this system is displayed in Fig. 1 based on a force-voltage mechanical-to-electrical analogy for the special case of quintic (fifth order) nonlinearity. Therefore, the force terms of Eq. (2a) are implemented as voltages that are the input or output of each block in Fig. 1. Although similar system level equivalent circuits for nonlinear electromechanically coupled systems have already been presented in the literature [5], this section discusses and presents electrical circuit solutions that allow for the practical implementation and experimental validations of such systems. Moreover, the equivalent electrical circuit of the current paper also enables the electrical representation of high quality factor systems by keeping low internal resistances for each sub-circuit (each block) of Fig. 1. The

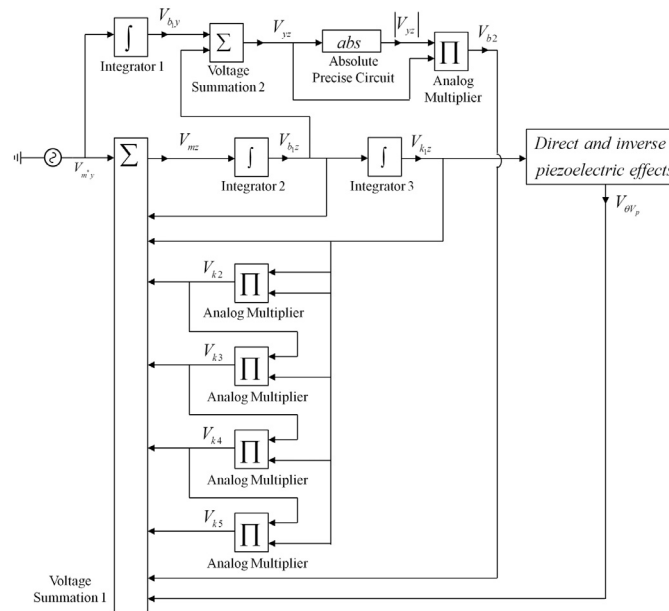


Fig. 1. Block diagram for the equivalent circuit representation of a nonlinear electromechanically coupled system (with a quintic stiffness nonlinearity).

following subsections describe the sub-circuits of Fig. 1.

2.1. Summing amplifier circuit

The block “Voltage Summation 1” of Fig. 1 is the basic summing amplifier circuit of Fig. 2. Therefore, in this sub-circuit, each input voltage is equivalent to each mechanical (or electromechanical) term of the right-hand side of Eq. (2a), while the output voltage is V_{mz} , that is the equivalent electrical of the force $m\ddot{z}$ of Eq. (2a). In particular, the input voltage V_{m*y} is the electrical equivalent of the applied force due to the base excitation of the nonlinear oscillator, which, in practice, can be obtained by using a waveform generator. All the other input voltages of the basic summing amplifier circuit are obtained from the other sub-

circuits to be discussed in the following subsections.

The voltage output (V_{mz}) of the summing amplifier is

$$V_{mz} = -R_f \left(\frac{V_{m*y}}{R_{s1}} + \frac{V_{b1z}}{R_{s2}} + \frac{V_{b2}}{R_{s3}} + \frac{V_{k1}}{R_{s4}} + \frac{V_{k2}}{R_{s5}} + \frac{V_{k3}}{R_{s6}} + \frac{V_{k4}}{R_{s7}} + \frac{V_{k5}}{R_{s8}} + \frac{V_{\theta V_p}}{R_{s9}} + \frac{V_o}{R_{s0}} \right) \quad (3)$$

where each resistor is displayed in Fig. 2, and the subscript of each voltage refers to a force term in Eq. (2a).

The summing circuit, as well as the other sub-circuits of Fig. 1, uses op-amps or integrated circuits (ICs) in order to accomplish its function and also to keep low internal resistance. Op-amps and analog ICs exhibit certain characteristics that must be considered in the circuit design: (i) they have a saturation voltage and (ii) they present distortions for low voltage levels (typically below 100 mV). Therefore, the voltage levels along the circuit should be smaller than the saturation and large enough for their proper operation. In this work, the voltage level of each equivalent voltage is controlled by a parameter β_i . Therefore, when performing the mechanical-to-electrical analogy, each force term of Equation (2) is multiplied by a constant β_i (i.e. $V_{m*y} = \beta_{m*y} m*\ddot{y}$, $V_{b1y} = \beta_{b1y} b_{1y}\dot{y}$ and so on). In practice, the effect is to amplify the voltage level in the circuit and, simultaneously, avoid the saturation of the components of each sub-circuit. The previous knowledge of force levels of the mechanical system to be represented by an equivalent electrical circuit (that will result in the voltage terms in the electrical domain) allows for the proper calculation of each constant, as discussed in the Appendix of this paper.

One should note, however, that the pre-multiplication of each term of Equation (2) by different constants is physically inconsistent. This issue is addressed through the proper calculation of the resistors in the summing circuit (as well as the calculation of the electrical elements of each sub-circuit in this paper, as will be discussed later). Each term of the right-hand-side of Eq. (3) that is divided by a summing resistor (from R_{s1} to R_{s9}) must be numerically equal to the right-hand side of Eq. (2a) in order to properly represent the mechanical system. In this way, considering a constant β_i multiplying each term of Eq. (2a), the resistors of the summing circuit are obtained as

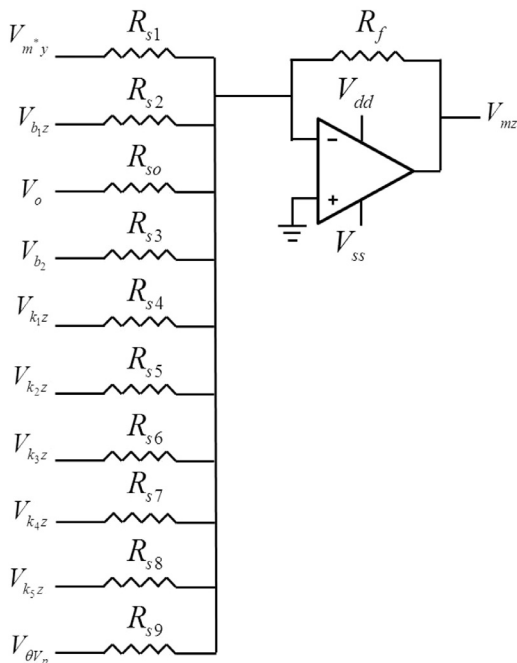


Fig. 2. Basic summing amplifier circuit.

$$\begin{aligned}
 R_{s1} &= R_f \frac{\beta_{m^*y}}{\beta_{mz}} & R_{s2} &= R_f \frac{\beta_{b1z}}{\beta_{mz}} & R_{s3} &= R_f \frac{\beta_{b2}}{\beta_{mz}} & R_{s4} &= R_f \frac{\beta_{k1}}{\beta_{mz}} & R_{s5} &= R_f \frac{\beta_{k2}}{\beta_{mz}} \\
 R_{s6} &= R_f \frac{\beta_{k3}}{\beta_{mz}} & R_{s7} &= R_f \frac{\beta_{k4}}{\beta_{mz}} & R_{s8} &= R_f \frac{\beta_{k5}}{\beta_{mz}} & R_{s9} &= R_f \frac{R_{k4}}{R_{x3} \theta \beta_{mz}}
 \end{aligned}
 \tag{4}$$

where R_f can be chosen arbitrarily. Note that Eq. (2a) is obtained when the summing resistors of Eq. (4) and the expression $V_{mz} = \beta_{mz} m \ddot{z}$ are used in Eq. (3), except for the last term of the right-hand-side of Eq. (3). Such term provides negative resistance effect in order to cancel the parasitic resistance (in the breadboard setting) usually observed in practical implementations. The summing resistor R_{s9} controls the amount of negative damping and can be determined from experimental tests, as will be discussed in Section 3.

2.2. Integrator circuit

The voltage V_{b1z} (that is equivalent to the linear damping force $b_1 \dot{z}$) and the voltage V_{k1z} (that is equivalent to the linear stiffness force $k_1 z$) are obtained from voltage term V_{mz} (that is the output of the summing circuit in Fig. 2). Fig. 3 shows the circuit of each integrator block (Integrator 1, Integrator 2 and Integrator 3) of Fig. 1. The subscript i stands for the index of the integrator block ($i = 1, 2$ or 3), V_{in} stands for the input voltage, while V_{out} stands for the output voltage of the block. Fundamental integrator circuits (with a capacitor C_i in the feedback loop of an inverter amplifier circuit) are employed for the time integration of V_{in} . The resistor R_{dci} is also added to avoid cumulative summing of the output voltage due to DC offset voltages at the input V_{in} . An inverting amplifier circuit is also included in each Integrator block to adjust the signal of V_{out} .

The resistors (R_1, R_2 and R_3) of each integrator circuit are calculated according to the input and output voltages of the integrator block. For example, when V_{m^*y} and V_{b1y} are, respectively, the input and output voltage of the block Integrator 1, the governing equation is

$$\begin{aligned}
 V_{out} &= V_{b1y} = \beta_{b1y} b_1 \dot{y} = \frac{1}{R_1} \frac{\omega R_{dci}}{\sqrt{1 + (\omega R_{dci} C_1)^2}} \int \beta_{m^*y} m^* \dot{y} dt \\
 &\cong \frac{1}{R_1 C_1} \int \beta_{m^*y} m^* \dot{y} dt
 \end{aligned}
 \tag{5}$$

for $\omega R_{dci} C_1 \gg 1$. The capacitor C_1 can be chosen arbitrarily and the resistor R_1 is calculated as

$$R_1 = \frac{\beta_{m^*y} m^*}{\beta_{b1y} b_1 C_1}
 \tag{6}$$

which takes into account each constant β and also the mass and damping coefficient of the mechanical terms. Therefore, the output of Eq. (5) is a voltage that is equivalent to a mechanical force.

By repeating the procedure of Eqs. (5) and (6) for the integrator 2 and 3, the resistors R_2 and R_3 can be calculated as

$$R_2 = \frac{\beta_{mz} m}{\beta_{b1z} b_1 C_2} \quad R_3 = \frac{\beta_{b1z} b_1}{\beta_{k1z} k_1 C_3}
 \tag{7}$$

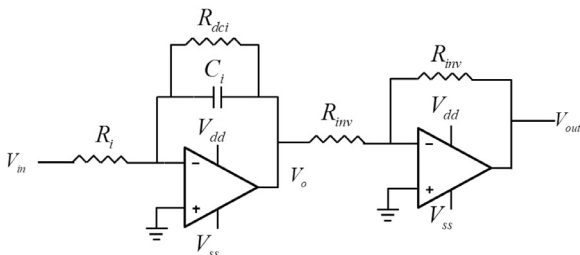


Fig. 3. Integrator circuit connected in series with an inverter amplifier to form the integrator block.

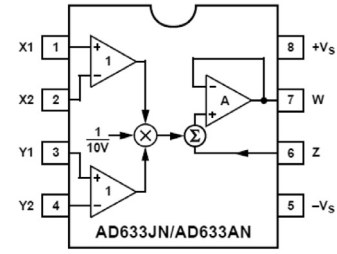


Fig. 4. Integrated component for multiplying two input voltages (from Analog Devices Inc.).

where the capacitors C_2 and C_3 can be chosen arbitrarily.

2.3. Circuits for nonlinear stiffness and nonlinear damping

The voltages V_{b1z} and V_{k1z} are the basis for the calculation of the nonlinear terms of Eq. (2a). The voltages V_{k2} , V_{k3} , V_{k4} , and V_{k5} are related to the nonlinear stiffness terms presented in Eq. (1b) and they are obtained by using a voltage multiplier. In this work, the integrated circuit AD633JN (from Analog Devices Inc.) shown in Fig. 4 is employed. In this IC, X and Y are differential voltage inputs and the output voltage W is given by

$$W = \frac{(X_1 - X_2)(Y_1 - Y_2)}{10} + Z
 \tag{8}$$

where Z is a voltage input used to provide a positive bias to the output. Therefore, the voltage V_{k2} (equivalent to the force related to the quadratic nonlinear stiffness of Eq. (1b)) is obtained when V_{k1z} is the input at X_1 and Y_1 while X_2, Y_2 and Z are grounded. The equivalent of the cubic stiffness (V_{k3}) is obtained when a second multiplier is combined to the first one (used to obtain the quadratic nonlinearity). In such case, the voltage output of the first multiplier (V_{k2}) is connected to the port X_1 of the second multiplier, while Y_1 remains connected to the voltage V_{k1z} . By continuously repeating this procedure, any power of z can be obtained (and note that a fifth-order polynomial would be obtained in the configuration presented in Fig. 1). Since the polynomial stiffness is of order 5 (quintic stiffness as in the experimental case in [33] to be visited in this work), four voltage multipliers are required to properly represent the nonlinear stiffness.

The electrical components for calculating the voltage equivalent to the nonlinear damping force (V_{b2}) are the block “Voltage Summation 2”, the block “Absolute precise circuit”, and an analog voltage multiplier. The sub-circuits inside the blocks “Voltage Summation 2” and “Absolute precise circuit” are shown Fig. 5a and b, respectively. The block “Voltage Summation 2” is composed of the op-amp OA1 and the resistors R_{s10} and R_{s11} . The resistors R_{s10} and R_{s11} along with the op-amp OA1 performs a weighted sum of the voltages V_{b1y} and V_{b1z} , resulting in the voltage term V_{yz} :

$$V_{yz} = \beta_{b1y} b_1 \dot{y} \frac{R_{s11}}{R_{s10} + R_{s11}} + \beta_{b1z} b_1 \dot{z} \frac{R_{s10}}{R_{s10} + R_{s11}}
 \tag{9}$$

and V_{yz} becomes proportional to $\dot{y} + \dot{z}$ by assuming $R_{s11} = \frac{\beta_{b1z}}{\beta_{b1y}} R_{s10}$. Note that R_{s10} can be chosen arbitrarily and R_{s11} is function of R_{s10} . Then, V_{yz} becomes

$$V_{yz} = \beta_{b1yz} b_1 (\dot{y} + \dot{z})
 \tag{10}$$

where

$$\beta_{b1yz} = \frac{\beta_{b1y} \beta_{b1z}}{\beta_{b1y} + \beta_{b1z}}
 \tag{11}$$

The voltage V_{yz} is driven to the precision absolute value circuit of Fig. 5b so that the voltage term $|V_{yz}|$ (proportional to $|\dot{y} + \dot{z}|$) can be obtained. This sub-circuit presents two semi-conductor components

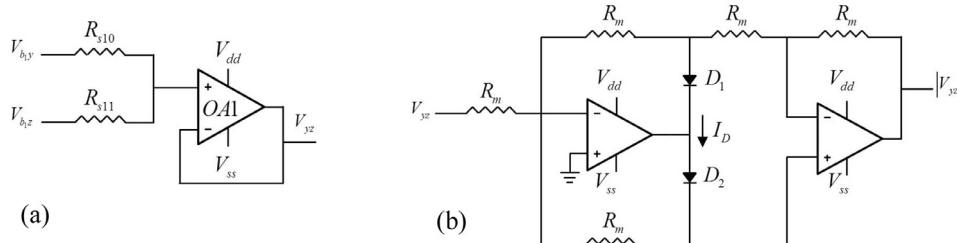


Fig. 5. Sub-circuits inside (a) the voltage summation 2 block and (b) the precision absolute value circuit used to calculate the modulus of an input voltage.

(diodes D_1 and D_2). The semi-conductor components present threshold values that undermine the precision of the circuit. However, the threshold effects are minimized when the current flowing through the diodes (I_D) is low, which is achieved by using high resistance values for R_m .

The voltages V_{yz} and $|V_{yz}|$ are then inputs to the analog multiplier (Fig. 4) and the output voltage V_{b2} (proportional to $(\dot{y} + \dot{z})|\dot{y} + \dot{z}|$) represents the nonlinear damping in the equivalent electrical circuit.

2.4. Circuit for electromechanical coupling

The equivalent electrical representation of the electromechanical coupling term of Eq. (2a) and the solution of Eq. (2b) are described next. Eq. (2a) states that the piezoelectric voltage V_p is given by a controlled voltage source ($V_s = -\theta z/C_p$) in series with a capacitor (C_p). The controlled voltage source stands for the piezoelectric coupling effect and can be represented by the two resistors R_{x1} and R_{x2} and the op-amp OA2, as shown in Fig. 6. Note that the circuit of Fig. 6 represents Eq. (2b) regardless of the electrical circuit connected to the piezoelectric material. As a result, this circuit topology with a novel representation of the direct and converse effects can be used in vibration control and energy harvesting problems conveniently without loss of accuracy. The inverting amplifier circuit composed of R_{x1}, R_{x2} and OA2 combines the voltage term V_{k1z} (equivalent to the linear stiffness) with the controlled voltage source V_s to generate the direct piezoelectric effect, such that

$$\frac{V_s}{V_{k1z}} = -\frac{R_{x2}}{R_{x1}} \tag{12}$$

and considering that $V_{k1z} = \beta_{k1z} k_1 z$ and $V_s = -\theta z/C_p$, the electromechanical coupling resistor R_{x2} can be written as

$$R_{x2} = R_{x1} \frac{\theta}{\beta_{k1z} k_1} \tag{13}$$

where R_{x1} can be chosen arbitrarily.

The mechanical force related to the converse piezoelectric effect of Eq. (2a) is represented by the voltage $V_{\theta V_p}$, that is calculated as

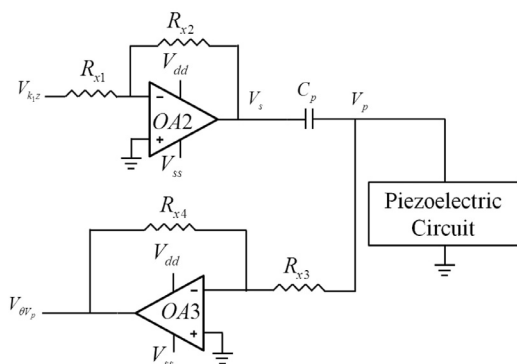


Fig. 6. Equivalent circuit representation of the direct and converse piezoelectric effects.

$$V_{\theta V_p} = -\frac{R_{x4}}{R_{x3}} V_p \tag{14}$$

which is obtained from the op-amp OA3 and the resistor R_{x3} and R_{x4} . Note that resistor R_{x3} is in parallel connection with the piezoelectric circuit block (voltage across R_{x3} is V_p and the electrical ground). Due to the parallel connection, the equivalent impedance observed by V_p never exceeds R_{x3} . Furthermore, resistor R_{x3} must be taken into account when designing a high impedance piezoelectric circuit (R_{x3} can be chosen arbitrarily as long as it assumes high values). The calculation of the resistor R_{x4} is based on the maximum values of V_p and $V_{\theta V_p}$ ($\max(V_{\theta V_p}) = V_{sat}$), according to

$$R_{x4} = R_{x3} \frac{V_{sat}}{\max(V_p)} \tag{15}$$

where the idea is that OA3 reaches the saturation (V_{sat}) when the maximum voltage output V_p from the piezoelectric material is reached. The voltage output from the piezoelectric material (V_p) is related to the application as well as the type of piezoelectric material considered.

Fig. 7 shows the complete equivalent circuit for an electromechanically coupled nonlinear oscillator with damping and stiffness nonlinearities. In the example of Fig. 7a, quintic restoring elastic force is considered, although nonlinearities of any order can be assumed depending on the number of multipliers.

3. Case studies and results

The goal of this work is to provide an equivalent electrical circuit representation (as well as its practical implementation) for high quality factor linear and nonlinear oscillators with piezoelectric coupling. Therefore, in this section, the equivalent electrical circuit obtained from the system-level analysis of Fig. 1 is implemented (built on breadboards) and employed to obtain the behavior of two different configurations. In the first case, a high quality factor SDOF mass-spring-damper system is considered. In such case, the system-level simulation is performed in MATLAB Simulink using the ODE45 solver. Experimental results obtained from the breadboard implementation of a linear version of the equivalent electrical circuit (Fig. 1) are validated against numerical results in time and frequency domains.

In the second case, the experimental results obtained from the equivalent electrical circuit for a nonlinear electromechanically coupled structure are validated against the numerical results and experimental data presented in the literature (Leadenham and Erturk [33]). The M-shaped piezoelectric structure (an energy harvester) is a high quality factor nonlinear oscillator with electromechanical coupling and a resistive electrical load. The equations of motion include quadratic damping and nonlinear (quintic) stiffness and are similar to the Equations (1) of the present work. Leadham and Erturk [33] provide detailed information concerning the nonlinear structure, modeling, and experimental results.

3.1. Linear structure

The structural parameters of the linear mass-spring-damper

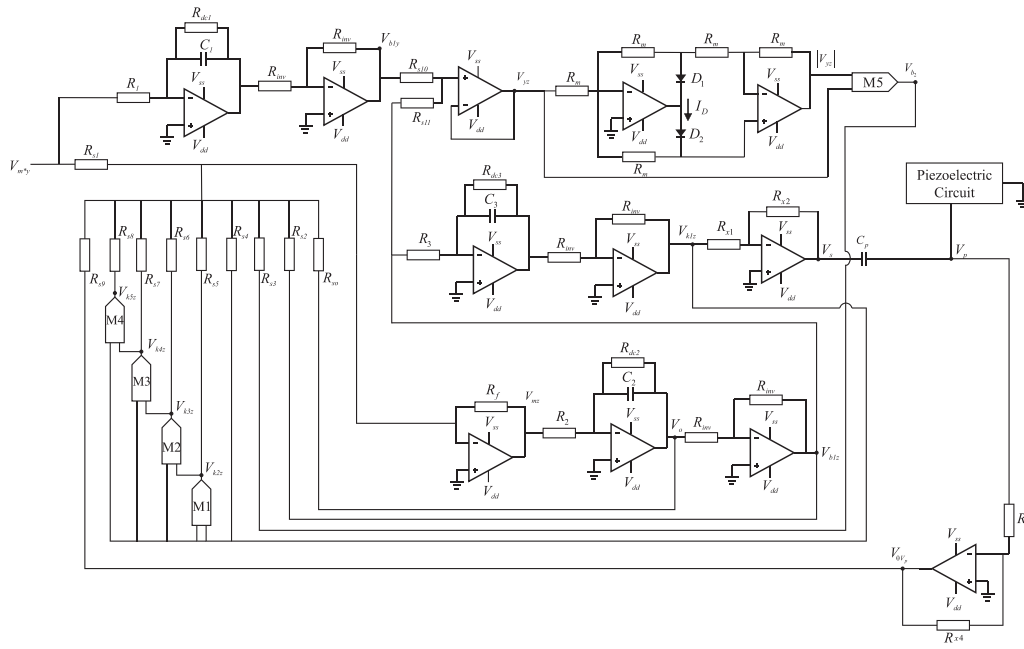


Fig. 7. Equivalent circuit for or an electromechanically coupled nonlinear oscillator with damping and stiffness nonlinearities.

mechanical system are shown in Table 1. The parameters were obtained from Leadenham and Erturk [33], excluding the nonlinear ones and also the electromechanical coupling (basically the system in this section is the linearized mechanical version of the M-shaped structure [33]). The natural frequency ($\omega_n = \sqrt{k_1/m}$), the quality factor (Q_f), and the damping ratio (ζ) of the mechanical system are shown in Table 1. In order to represent the linear mechanical system, the equivalent circuit of Fig. 1 is modified. In such case, the resistors R_{s3} , R_{s5} , R_{s6} , R_{s7} , R_{s8} and R_{s9} are set considerably high ($10^9\Omega$) in the numerical simulations. In the experimental tests (on a breadboard), those resistors are removed from the circuit. The value of each electrical component of the circuit to reproduce the linear structure is shown in Table 2, following the discussion of Section 2 in this paper. The LM358P op-amps were used in the circuit and symmetrical voltage supplies of $\pm 14V$ were employed during the tests. For calculation of the resistors, a safety factor $\alpha = 0.9$ was assumed and the saturation voltage of the analog voltage multiplier AD633JN ($V_{sat} = 10V$) was used as reference for all components of the circuit (even though the LM358P has higher saturation voltage).

In the simulations, an RMS (root-mean-square) base acceleration of 0.04 g was assumed. This excitation level corresponds to an input voltage (term V_{m^*} , in Fig. 1) of 9 V in the equivalent electrical circuit. The voltage outputs V_{mz} , V_{b1z} and V_{k1z} were measured experimentally and data acquisition performed with a Siemens Scadas Mobile system. The acquired voltages are then divided by $\beta_{mz}m$, $\beta_{b1z}b_1$ and $\beta_{k1z}k_1$, respectively, so the experimental values of ζ , \bar{z} and z could be obtained.

3.1.1. Parasitic damping

As discussed in Section 2, the voltage V_o provides negative damping to the system in order to cancel the parasitic damping (resistance) of breadboards and/or electrical components. The summing resistor R_{s0} controls the amount of negative damping provided by V_o . The experimental tests to determine R_{s0} are divided in three steps: (1) In the first step, the resistor R_{s2} (related to linear damping) is removed from the

Table 1 Parameters of the linear mechanical system (linearized structure).

$m(g)$	$b_1(Nsm^{-1})$	$k_1(Nm^{-1})$	$\omega_n(Hz)$	Q_f	ζ
31.9	5.5×10^{-3}	244.1	13.92	504.7	0.001

Table 2

Parameters of the electrical components used in the equivalent circuit representation of the linear mechanical system.

R_2 37.0 k Ω	R_3 45.27 k Ω	C_2 224 nF	C_3 224 nF	R_{dc2}, R_{dc3} 100 M Ω
R_{inv} 1.0 M Ω	R_{s1} 210 k Ω	R_{s2} 640 k Ω	R_{s4} 1.3 k Ω	R_f 1.0 k Ω

circuit and a resistance box is used for R_{s0} . The initial value of R_{s0} is set to be very high (10M Ω) and, therefore, no negative damping is provided. The voltage excitation V_{my} is applied for a couple of seconds and then removed in order to measure the free response of the equivalent electrical circuit. The decaying behavior observed in the free response (at the natural frequency of the system) of the voltage terms V_{k1z} , V_{b1z} and V_{mz} provides the amount of parasitic damping (calculated as $\zeta = 0.0013$) of the electrical circuit and breadboard. (2) The second step consists of slowly reducing the resistance value of R_{s0} . A decrease in R_{s0} means an increase of the negative damping added to the system. When the negative damping cancels the parasitic damping, the free response of V_{k1z} , V_{b1z} and V_{mz} presents constant amplitude and the empirical value of R_{s0} is obtained (472k Ω). (3) The third step is a validation step. In this case, the resistor R_{s2} is replaced in the circuit along with the empirical value of R_{s0} obtained in the second step. The resulting decay rate of V_{k1z} , V_{b1z} and V_{mz} must match the decay rate shown in Table 1. Fig. 8 shows the normalized displacement ($\bar{z} = z/\max(z)$) obtained experimentally from the equivalent circuit during each step.

3.1.2. Numerical and experimental results

Having obtained the required resistance to minimize the parasitic damping, the experimental results (from the breadboard implementation of the equivalent electrical circuit) are validated against numerical results obtained by solving the equation of motion of the SDOF mechanical system under base excitation in Simulink (using the solver ODE45). Fig. 9 to 11 show the displacement z of the system when the system is excited at 13.50 Hz, 13.92 Hz (resonance frequency) and 14.50 Hz. In the experiments, the excitation voltage V_{m^*} for each case was 9 V, 3 V, and 9 V, respectively. The excitation voltage of 3 V was used in the resonance condition of Fig. 10 to avoid the saturation of the op-amps. Very good agreement is observed between numerical and

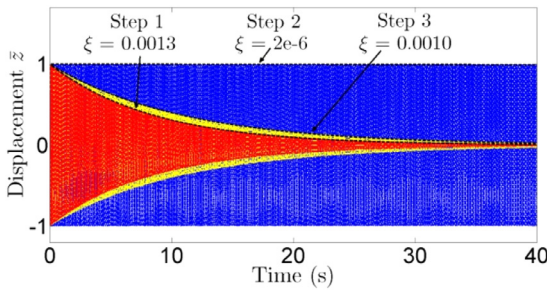


Fig. 8. Experimental results for the dimensionless displacement in the equivalent electrical circuit emulating the linear mechanical system.

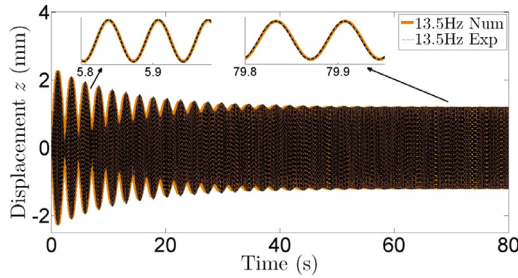


Fig. 9. Numerical and experimental results obtained from the equivalent electrical representation of the linear mechanical system when the system is excited at 13.50 Hz.

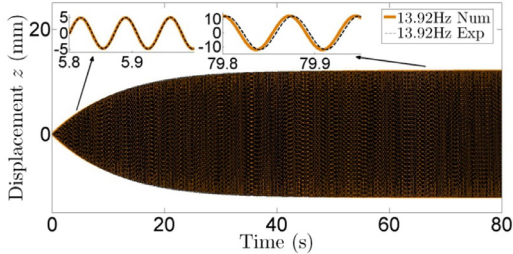


Fig. 10. Numerical and experimental results obtained from the equivalent electrical representation of the linear mechanical system when the system is excited at 13.92 Hz.

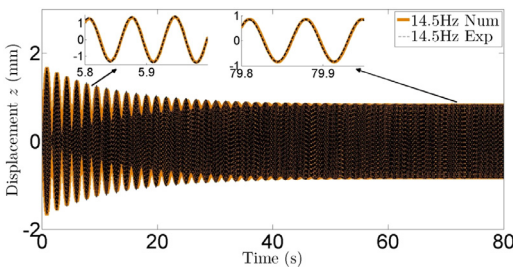


Fig. 11. Numerical and experimental results obtained from the equivalent electrical representation of the linear mechanical system when the system is excited at 14.50 Hz.

experimental data during transient and steady state responses at different frequencies.

Fig. 12 shows the numerical and experimental mechanical vibration frequency response functions (mass displacement to base acceleration FRF) of the linear structure over the frequency range of 13 Hz to 15.5 Hz. A chirp signal (V_{m^*y}) was employed to excite the equivalent circuit in the experiments over a range of frequencies from 12 Hz and 16.5 Hz. The amplitude of V_{m^*y} is 3 V in order to avoid saturation of the op-amps. Fig. 13 displays the coherence for the same FRF measured

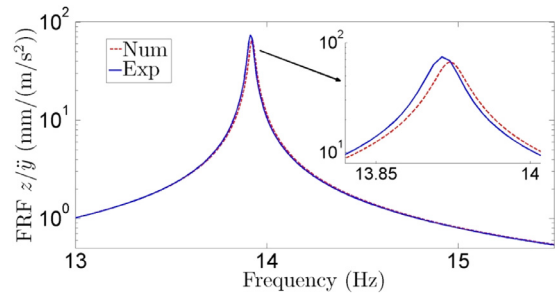


Fig. 12. Numerical and experimental frequency response results obtained from the equivalent electrical representation of the linear mechanical system.

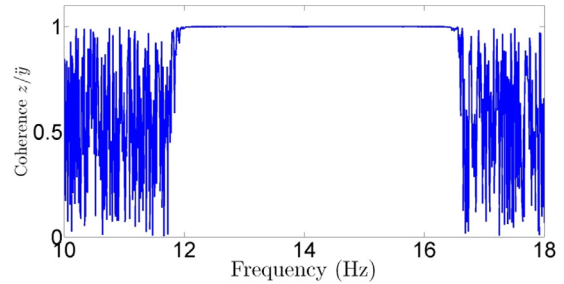


Fig. 13. Experimental coherence associated with the equivalent electrical representation of the linear mechanical system.

during the experiments.

In Fig. 12, the experimental resonance slightly deviates from the numerical one, which can be observed in the close-up view of Fig. 12. The experimental resonance frequency is 0.07% lower than the numerical one, while the amplitude at the experimental resonance frequency is 10% larger than the numerical one. The value of each electrical component of the circuit employed in the experiments (Table 2) was calculated by following the discussion of Section 2. However, commercially available resistors and capacitors may have capacitances and resistances slightly different from the calculated ones due to their manufacturing tolerance (i.e. resistors with tolerance of 2% were employed). Moreover, in practice, op-amps are not ideal electrical elements (as assumed in simulations) since they present output resistance. Therefore, the stiffness and damping values obtained in the experimental circuit slightly differ from the values used in the simulations, leading to differences between numerical and experimental results. In particular, small damping variations leads to significant amplitude variations around the resonance frequency of high quality factor systems ($Q = 504.7$ in the discussed case). Nonetheless, the overall agreement in Fig. 12 is very good.

3.2. Nonlinear electromechanically coupled M-shaped structure

In this section, the experimental results obtained from the equivalent electrical circuit representation for the electromechanically coupled M-shaped structure are validated against the numerical results presented in the literature [33]. Leadenhams and Erturk [33] used the method of harmonic balance to obtain the steady state solution of the electromechanically coupled M-shaped harvester under base excitation. Table 3 presents the experimentally identified parameters [33] which are also used in the present paper to obtain the equivalent electrical parameters.

In their numerical simulations, Leadenhams and Erturk [33] considered a set of five load resistances (30kΩ, 100kΩ, 300kΩ, 1MΩ and 3MΩ). For the experiments with the equivalent electrical circuit, the same set of load resistances are of interest. However, it is important to note that R_{piezo} (the resistor used in the “piezoelectric circuit” block of Fig. 6) is in parallel connection with the resistor R_{x3} . The equivalent

Table 3
Mechanical, electrical, and electromechanical parameters of the M-shaped structure.

$m(g)$	$b_1(Nsm^{-1})$	$k_1(Nm^{-1})$	$\theta(NV^{-1})$	$C_p(nF)$	$k_2(Nm^{-2})$
31.9	5.5×10^{-3}	244.1	170×10^{-6}	34.27	2680
$k_3(Nm^{-3})$	$k_4(Nm^{-4})$	$k_5(Nm^{-5})$	$b_2(Nm^{-2}/s^{-2})$	$\omega_n(Hz)$	ξ
363×10^3	10.6×10^6	210×10^6	0.012	13.92	0.0010

Table 4
Electrical components used in the equivalent circuit to represent the nonlinear M-shaped structure.

R_1	R_2	R_3	C_1	C_2	C_3
1.6 M Ω	37.0 k Ω	45.27 k Ω	6.8 nF	224 nF	224 nF
R_{dc1}	R_{dc2}, R_{dc3}	R_{inv}	R_m	R_f	R_{s0}
1.61 M Ω	100 M Ω	1.0 M Ω	1.0 M Ω	1.0 k Ω	472 k Ω
R_{s1}	R_{s2}	R_{s3}	R_{s4}	R_{s5}	R_{s6}
210 k Ω	640 k Ω	245.6 k Ω	1.3 k Ω	9.04 k Ω	5.10 k Ω
R_{s7}	R_{s8}	R_{s9}	R_{s10}	R_{s11}	R_{x1}
13.72 k Ω	51.38 k Ω	110 k Ω	10 M Ω	58.18 k Ω	100 k Ω
R_{x2}	R_{x3}	R_{x4}	C_p		
649.6 k Ω	10 M Ω	450 k Ω	34.17 nF		

resistance (R_{eq}) between R_{piezo} and R_{x3} must match the values of the set of load resistances considered in [33]. The following values for R_{piezo} are used in the experiments with the equivalent electrical circuit: 30k Ω , 101k Ω , 309.2k Ω , 1.11M Ω and 4.286M Ω .

Table 4 displays all the electrical elements employed in the practical implementation of the equivalent electrical circuit of the M-shaped structure. The LM358P op-amps were used in the circuit and symmetrical voltage supplies of ± 14 V were employed during the tests. A safety factor $\alpha = 0.9$ and a saturation voltage $V_{sat} = 10V$ were assumed. Diodes of BYW95C type were used in the equivalent circuit.

Fig. 14 presents the mechanical and electrical outputs of the electromechanically coupled M-Shaped harvester for the set of load resistances. The continuous lines stand for the numerical results of Leadenham and Erturk [33] while the dashed lines with markers are the experimental results obtained from the equivalent circuit of the present paper on a breadboard. In the experiments, the input voltage ($V_{m\gamma}$) of

the equivalent electrical circuit was a sine sweep with frequency step of 0.05 Hz (60 s for each frequency). The amplitude of the input voltage was 9 V which is equivalent to the RMS base acceleration of 0.04 g reported in [33]. Up and down frequency sweeps were performed in order to capture the jump phenomenon associated with bifurcations of the nonlinear M-Shaped structure.

A very good agreement is observed between numerical predictions and experimental results (from the equivalent circuit) for the absolute velocity output ($\dot{y} + \dot{z}$) of the system as well as for the electrical outputs of the piezoceramic material (voltage output, electrical current, and power). Although the experimental results from the equivalent circuit slightly underestimate the amplitudes of numerical responses (for the reasons discussed with Fig. 12), the experimental results exhibit the same trends observed in the numerical ones. The velocity response shows that damping due to load resistance increases from short circuit condition until 300k Ω and then decreases as the load resistance is increased. Therefore, 300k Ω is the optimum load (among the ones considered) that leads to the maximum shunt damping effect that results in the shortest nonlinear frequency bandwidth (frequency range with simultaneous high and low amplitudes solution) in both numerical predictions and experimentally measured responses. The same trend is observed in electrical responses of Fig. 14b–d. Additionally, voltage increases with increasing load resistance, while electrical current decreases with increasing load resistance. The optimal load resistance of 300k Ω also provides the largest power output as shown in Fig. 14d.

Leadenham and Erturk [33] report a bandwidth of 0.38 Hz for the load resistance of 300 k Ω . The calculated bandwidth from the experimental results for the same load is in between 0.35 Hz and 0.40 Hz (since the experimental input voltage was a sine sweep with frequency step of 0.05 Hz), revealing a good agreement between the experimental and numerical results.

After validating the equivalent electrical circuit against numerical results presented in the literature for a nonlinear electromechanical structure (Fig. 14), the experimental nonlinear voltage terms (similar to linear and nonlinear stiffness and nonlinear damping of the system) are now used to discuss the behavior of the nonlinear oscillator. Fig. 15 shows the nonlinear voltage terms ($V_{k2}, V_{k3}, V_{k4}, V_{k5}$ and V_{b2}) along with the voltage related to the linear stiffness V_{k1z} that were experimentally obtained from the equivalent electrical circuit of the nonlinear M-shaped structure (during the same experimental tests to obtain the results shown in Fig. 14). Additionally, Fig. 15 also displays the noise floor level (or the minimum required input signal level) of the analog

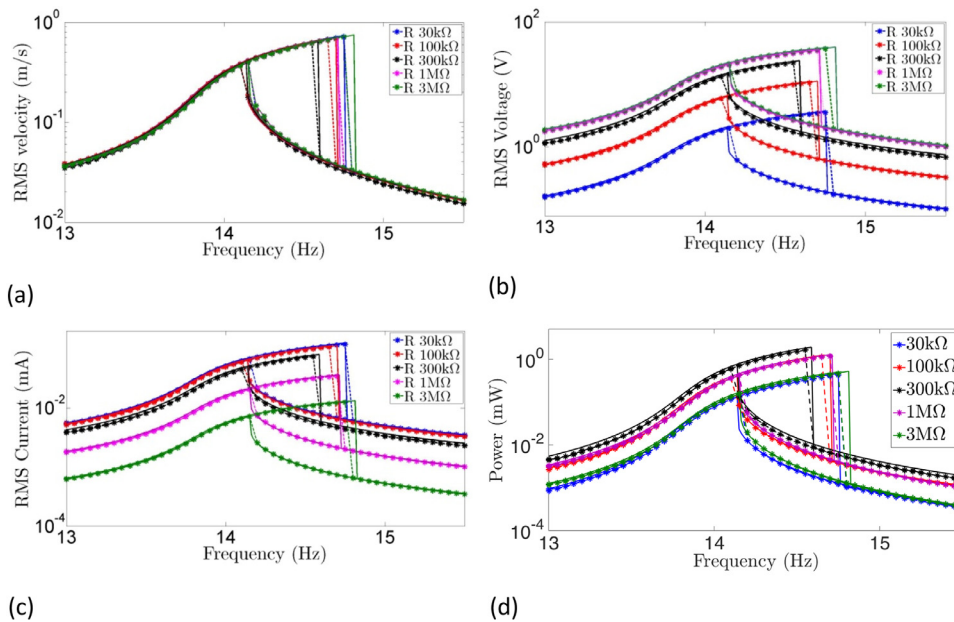


Fig. 14. Numerical (continuous lines) and experimental (dashed lines with markers) frequency domain results obtained from the equivalent electrical representation of the nonlinear M-shaped structure in the neighborhood of the primary resonance for various forms of the response: (a) Velocity, (b) voltage, (c) current, and (d) electrical power.

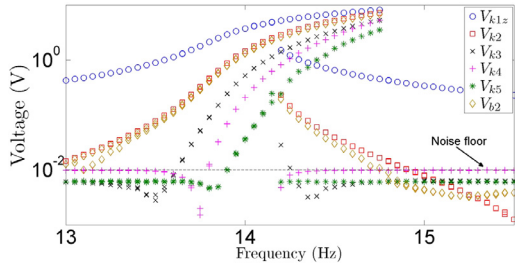


Fig. 15. Frequency behavior of the nonlinear voltage terms (V_{k2} , V_{k3} , V_{k4} , V_{k5} and V_{b2}).

voltage multipliers used in the nonlinear equivalent circuit. Only voltages larger than the noise floor level contribute to the behavior of the system.

Fig. 15 shows that the voltage equivalent to the linear stiffness, V_{k1z} , remains far above the noise floor level throughout the entire range of frequencies (from 13 Hz to 15.5 Hz). On the other hand, the behavior of the nonlinear voltage terms is significantly different. They are only above the noise floor level at frequencies around the linear resonance frequency of the M-shaped structure (close to 13.9 Hz for the short circuit condition) and below the noise floor level for frequencies significantly smaller or significantly larger than the resonance frequency. Therefore, linear and nonlinear terms contribute to the system behavior around the resonance (where dominant hardening nonlinearity and jump phenomenon are observed) while the linear term is the most significant one at off-resonance frequencies. In practice, as one moves away from the resonance condition, the displacement z of the mechanical M-shaped structure (governed by Equations (1)) decreases. Since the equivalent voltages V_{k2} and also V_{b2} , V_{k3} , V_{k4} , and V_{k5} decrease proportionally to z^2 , z^3 , z^4 and z^5 , respectively, the voltage terms representing the higher-order polynomial present a higher voltage drop in off-resonance regions. Fig. 15 also shows that the high-amplitude branch is due to a combination of all voltages (or all linear and nonlinear mechanical terms).

4. Conclusions

This paper presents a novel equivalent electrical circuit framework for electromechanically coupled linear and nonlinear systems with a focus on piezoelectric structures. The proposed linear and nonlinear equivalent circuit framework can easily represent high quality factor mechanical systems for applications spanning from energy harvesting

Supplementary materials

Supplementary material associated with this article can be found, in the online version, at [doi:10.1016/j.mechatronics.2018.07.009](https://doi.org/10.1016/j.mechatronics.2018.07.009).

Appendix. Adjustment of the voltage level

For the proper operation of the circuit in Fig. 1, all op-amps and analog IC devices must generate high output voltages that do not exceed the saturation level. Then, each voltage output shown in Fig. 1 is given by

$$\begin{aligned}
 V_{m^*y} &= \beta_{m^*y} m^* \ddot{y} & V_{b1y} &= \beta_{b1y} b_{1y} \dot{y} \\
 V_{mz} &= \beta_{mz} m \ddot{z} & V_{b1z} &= \beta_{b1z} b_{1z} \dot{z} \\
 V_{k1z} &= \beta_{k1z} k_1 z & V_{k2} &= \beta_{k2} k_2 z^2 \\
 V_{k3} &= \beta_{k3} k_3 z^3 & V_{k4} &= \beta_{k4} k_4 z^4 \\
 V_{k5} &= \beta_{k5} k_5 z^5 & V_{b2} &= \beta_{b2} b_2 (\dot{y} + \dot{z}) \dot{y} + \dot{z}
 \end{aligned} \tag{16}$$

where β_{m^*y} , β_{b1y} , β_{mz} , β_{b1z} , β_{k1z} , β_{k2} , β_{k3} , β_{k4} , β_{k5} , and β_{b2} are proportionality coefficients. The purpose of these coefficients is to amplify the voltage output of op-amps and analog IC even if the force terms (of a mechanical system) presents low levels.

The value of the coefficients can be obtained based on the frequency response of the force term of Equation (1). As an example, Fig. 16 shows the frequency response of a system with predominant hardening effect. The maximum value of each force term is highlighted in this figure, while f_{ri} and f_{rf} represent the frequency bandwidth of interest in the system.

to vibration control. Most of the existing equivalent circuits reported in the literature are RLC arrangements to represent mass, damping and stiffness of electromechanical systems, while ideal transformers represent the electromechanical coupling. Although such configurations are widely employed for numerical analysis in circuit simulation software, their experimental implementations are not trivial. Especially in the particular case of high quality factor mechanical systems, the equivalent internal resistance of RLC circuits is usually large and ideal transformers or dependent sources cannot be easily obtained in an experimental circuit setting. The equivalent circuit approach proposed in this work overcomes such issues by eliminating the need for lossless ideal circuit components to represent a given linear or nonlinear electromechanical system.

The proposed equivalent circuit framework makes use of simple analog components such as resistors, integrated circuits (operational amplifiers and voltage multipliers), diodes and capacitors. Details for the practical implementation of the circuit are provided, which includes the electrical representation of stiffness and damping nonlinearities as well as a new approach to represent the electromechanical coupling (using operational amplifiers) of the system.

The equivalent circuit is validated for two different cases. In the first one, the equivalent electrical circuit of a high quality factor linear mechanical system is investigated. Experimental results obtained from a breadboard implementation of the equivalent circuit show good agreement with numerical results from system-level simulations. In the second case study, the equivalent electrical representation of a high quality factor nonlinear electromechanically coupled system (a nonlinear piezoelectric energy harvester) is discussed. Nonlinear stiffness and nonlinear damping are considered in the circuit representation together with the new op-amp-based representation of the electromechanical coupling. Experimental results obtained from breadboard implementation of the equivalent circuit are successfully validated against published data from the literature. The proposed equivalent nonlinear circuit and electromechanical system framework paves the way for the design, analysis, and experimental realization of electrical circuits emulating nonlinear structures, such as nonlinear vibration absorbers and energy sinks.

Acknowledgments

The authors gratefully acknowledge the support from CAPES (99999.003755/2015-00), from CNPq (402160/2013-4) and from FAPESP (2015/11325-3) for funding this project.

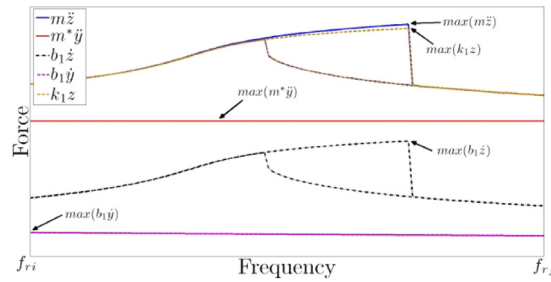


Fig. 16. Frequency response of a nonlinear system with the maximum value of the linear force term highlighted.

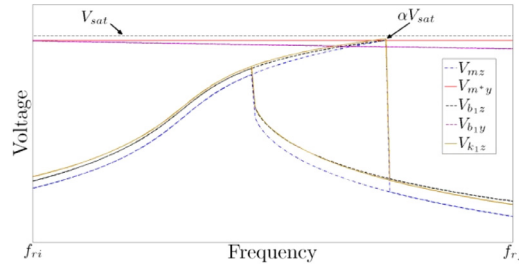


Fig. 17. Amplified voltage outputs (note that all voltage terms present high voltage output and never exceed the saturation voltage level).

The coefficients β_{m^*y} , β_{b_1y} , β_{mz} , β_{b_1z} , and β_{k_1z} are defined based on the maximum value of each force term ($m^*\ddot{y}$, $b_1\dot{y}$, $m\ddot{z}$, $b_1\dot{z}$ and k_1z) such that,

$$\begin{aligned} \beta_{m^*y} &= \frac{\alpha V_{sat}}{\max(m^*\ddot{y})} & \beta_{b_1y} &= \frac{\alpha V_{sat}}{\max(b_1\dot{y})} \\ \beta_{mz} &= \frac{\alpha V_{sat}}{\max(m\ddot{z})} & \beta_{b_1z} &= \frac{\alpha V_{sat}}{\max(b_1\dot{z})} \\ \beta_{k_1z} &= \frac{\alpha V_{sat}}{\max(k_1z)} \end{aligned} \tag{17}$$

where V_{sat} is the saturation voltage, α is a safety factor ($0 < \alpha < 1$) used to ensure the op-amps and the analog IC components do not reach the saturation level, and $\max(\cdot)$ is the maximum value assumed by the mechanical term of Eq. (1a) in the frequency response shown in Fig. 17. The coefficients β_{k_2} , β_{k_3} , β_{k_4} , β_{k_5} , and β_{b_2} are obtained as a function of the coefficients β_{k_1z} , β_{b_1z} and β_{b_1y} , such that

$$\beta_{k_i} = \frac{\beta_{k_{i-1}}k_{i-1}\beta_{k_1z}k_1}{10k_i} \tag{18a}$$

$$\beta_{b_2} = \frac{(\beta_{b_1z}b_1)^2}{10b_2} \tag{18b}$$

Note that the coefficients β_{k_2} , β_{k_3} , β_{k_4} , β_{k_5} , and β_{b_2} result from Eq. (9) of the analog voltage multiplier IC AD633JN, while the coefficient β_{b_1z} results from the summation performed by the electrical components R_{s10} , R_{s11} , and the op-amp OA1 (Fig. 5a). Fig. 17 shows the amplified voltage output (using coefficients β) for each term equivalent to the mechanical forces. As can be observed, the voltage terms V_{m^*y} , V_{b_1y} , V_{mz} , V_{b_1z} , and V_{k_1z} present same maximum value (αV_{sat}). Although the nonlinear voltage terms V_{k_2} , V_{k_3} , V_{k_4} , V_{k_5} , and V_{b_2} are not shown in Fig. 17 (for clarity), they have similar maximum voltage levels.

References

- [1] Moheimani SOR, Fleming AJ. Piezoelectric transducers for vibration control and damping. London: Springer; 2006.
- [2] Moheimani S. A survey of recent innovations in vibration damping and control using shunted piezoelectric transducers. IEEE Trans Control Syst Technol 2003;11:482–94.
- [3] Elvin N, Elvin A. A general equivalent circuit model for piezoelectric generators. J Intell Mater Syst Struct 2009;20:3–9.
- [4] Elvin N, Elvin A. A coupled finite element-circuit simulation model for analyzing piezoelectric energy generators. J Intell Mater Syst Struct 2009;20:587–95.
- [5] Elvin N. Equivalent electrical circuits for advanced energy harvesting. J Intell Mater Syst Struct 2014;25:1715–26.
- [6] B. Bayik, A. Aghakhani, I. Basdogan, A. Erturk, Equivalent circuit modeling of a piezo-patch energy harvester on a thin plate with AC–DC conversion - IOPscience, (2016).
- [7] Roundy S, Wright PK, Rabaey JM. Energy scavenging for wireless sensor networks : with special focus on vibrations. Boston: Kluwer Academic Publishers; 2004.
- [8] Erturk A, Inman DJ. Piezoelectric energy harvesting. Chichester: Wiley; 2011.
- [9] Elvin N, Erturk A. Advances in energy harvesting methods. Springer; 2013.
- [10] Roundy S, Wright PK, Rabaey J. A study of low level vibrations as a power source for wireless sensor nodes. Comput Commun 2003;26:1131–44.
- [11] Dutoit N, Wardle B. Experimental verification of models for microfabricated piezoelectric vibration energy harvesters. AIAA J 2007;45:1126–37.
- [12] Erturk A, Inman D. An experimentally validated bimorph cantilever model for piezoelectric energy harvesting from base excitations. Smart Mater Struct 2009;18.
- [13] De Marqui C, Erturk A, Inman D. An electromechanical finite element model for piezoelectric energy harvester plates. J Sound Vib 2009;327:9–25.
- [14] C. Williams, R. Yates, Analysis of a micro-electric generator for microsystems, 52 (1996) 8–11.
- [15] Arnold DP. Review of microscale magnetic power generation. IEEE Trans Magn 2007;43:3940–51.
- [16] Glynne-Jones P, Tudor M, Beeby S, White N. An electromagnetic, vibration-

- powered generator for intelligent sensor systems. *Sens Actuata A Phys* 2004;110:344–9.
- [17] Beeby S, Torah R, Tudor M, Glynn-Jones P, O'Donnell T, Saha C, Roy S. A micro electromagnetic generator for vibration energy harvesting. *J Micromech Microeng* 2007;17:1257–65.
- [18] Mann BP, Sims ND. Energy harvesting from the nonlinear oscillations of magnetic levitation. *J Sound Vib* 2009;319:515–30.
- [19] Mitcheson PD, Miao P, Stark BH, Yeatman EM, Holmes AS, Green TC. MEMS electrostatic micropower generator for low frequency operation. *Sens Actuata A Phys* 2004;115:523–9.
- [20] Le C, Halvorsen E, Sorasen O, Yeatman E. Microscale electrostatic energy harvester using internal impacts. *J Intell Mater Syst Struct* 2012;23:1409–21.
- [21] Anton S, Sodano H. A review of power harvesting using piezoelectric materials (2003-2006). *Smart Mater Struct* 2007;16:R1–21.
- [22] Cook-Chennault K, Thambi N, Sastry A. Powering MEMS portable devices - a review of non-regenerative and regenerative power supply systems with special emphasis on piezoelectric energy harvesting systems. *Smart Mater Struct* 2008;17.
- [23] Priya S. Advances in energy harvesting using low profile piezoelectric transducers. *J Electroceram* 2007;19:167–84.
- [24] Daqaq M, Masana R, Erturk A, Quinn D. On the role of nonlinearities in vibratory energy harvesting: a critical review and discussion. *Appl Mech Rev* 2014;66.
- [25] Stanton S, McGehee C, Mann B. Reversible hysteresis for broadband magnetopiezoelectric energy harvesting. *Appl Phys Lett* 2009;95.
- [26] Erturk A, Hoffmann J, Inman D. A piezomagnetoelastic structure for broadband vibration energy harvesting. *Appl Phys Lett* 2009;94.
- [27] Arrieta A, Hagedorn P, Erturk A, Inman D. A piezoelectric bistable plate for nonlinear broadband energy harvesting. *Appl Phys Lett* 2010;97.
- [28] Sneller A, Cette P, Mann B. Experimental investigation of a post-buckled piezoelectric beam with an attached central mass used to harvest energy. *Proc Inst Mech Eng [I]* 2011;225:497–509.
- [29] Tang L, Yang Y, Soh C. Toward broadband vibration-based energy harvesting. *J Intell Mater Syst Struct* 2010;21:1867–97.
- [30] Pellegrini S, Tolou N, Schenk M, Herder J. Bistable vibration energy harvesters: a review. *J Intell Mater Syst Struct* 2013;24:1303–12.
- [31] Harne R, Wang K. A review of the recent research on vibration energy harvesting via bistable systems. *Smart Mater Struct* 2013;22.
- [32] Leadenham S, Erturk A. M-shaped asymmetric nonlinear oscillator for broadband vibration energy harvesting: harmonic balance analysis and experimental validation. *J Sound Vib* 2014;333:6209–23.
- [33] Leadenham S, Erturk A. Nonlinear M-shaped broadband piezoelectric energy harvester for very low base accelerations: primary and secondary resonances. *Smart Mater Struct* 2015;24.
- [34] Shu Y, Lien I. Analysis of power output for piezoelectric energy harvesting systems. *Smart Mater Struct* 2006;15:1499–512.
- [35] Ottman G, Hofmann H, Bhatt A, Lesieutre G. Adaptive piezoelectric energy harvesting circuit for wireless remote power supply. *IEEE Trans Power Electron* 2002;17:669–76.
- [36] Ottman G, Hofmann H, Lesieutre G. IEEE, Optimized piezoelectric energy harvesting circuit using step-down converter in discontinuous conduction mode. *Pesc'02: 2002 IEEE 33rd Annual Power Electronics Specialists Conference, Vols 1-4, Conference Proceedings. 2002. p. 1988–94.*
- [37] Guyomar D, Badel A, Lefeuvre E, Richard C. Toward energy harvesting using active materials and conversion improvement by nonlinear processing. *IEEE Trans Ultrason Ferroelect Frequency Control* 2005;52:584–95.
- [38] Guyomar D, Richard C. Non-linear and hysteretic processing of piezoelement: Application to vibration control, wave control and energy harvesting. *Int J Appl Electromagnet Mech* 2005;21:193–207.



Mr. Tarcisio Marinelli Pereira Silva is a PhD candidate working at the Laboratory of Aeroelasticity and Smart Materials of the Sao Carlos School of Engineering, University of Sao Paulo, Brazil. Tarcisio obtained his master's and bachelor's degrees from the University of São Paulo and had a one-year internship at Airbus Operation SAS, in Toulouse, France. He also visited the Smart Structures and Dynamical Systems Laboratory of Georgia Tech for one year. Tarcisio has published papers in journals and conferences proceedings on topics including piezoelectric based vibration energy harvesting, vibration control, structural dynamics, analog and digital circuit design.



Mr. Marcel Araujo Clementino is a PhD candidate working at the Laboratory of Aeroelasticity and Smart Materials of the Sao Carlos School of Engineering, University of Sao Paulo, Brazil. He visited the Rotorcraft Research Group of Carleton University, Canada, for one year. Marcel has published papers in journals and conferences proceedings on topics including piezoelectric based vibration energy harvesting, vibration control, structural dynamics, and helicopters vibration control systems.



Alper Erturk is an Associate Professor and Woodruff Faculty Fellow in the G. W. Woodruff School of Mechanical Engineering at Georgia Institute of Technology, where he leads the Smart Structures and Dynamical Systems Laboratory. He has published 2 books and 200 papers in journals and conference proceedings on topics spanning from vibration energy harvesting and bio-inspired actuation to elastic/acoustic metamaterials and phononic crystals. He is a recipient of various awards including an NSF CAREER Award (2013), an ASME Gary Anderson Early Achievement Award (2015), and an ASME C.D. Mote Jr. Early Career Award (2017), among others. Dr. Erturk is a Fellow of ASME.



Carlos De Marqui Junior is an Associate Professor in the Department of Aeronautical Engineering of the Sao Carlos School of Engineering, University of Sao Paulo, Brazil. He has published book chapters, journal and conference papers on topics including linear and nonlinear aeroelasticity, smart materials and structures, energy harvesting, vibration control, and smart and adaptive elastic metamaterials. He is member of the Brazilian Society of Mechanical Sciences and Engineering (ABCM) and member of ASME.